Capturing 3D Temperature and Strain Fields using OBR-Based Sensing in AM Parts

Brian M. Hlifka, Robert G. Landers Edward C. Kinzel
Department of Aerospace and Mechanical Engineering, University of Notre Dame,
Notre Dame, IN 46556

Claire Henderson, Julin Wan, Thomas Adcock, Thomas Dyson, Victor Ostroverkhov, Laura Dial, Glen Koste, Gautam Parthasarthy
GE Research

Abstract

In-situ temperature and stress monitoring are critical for preventing part failure and enabling performance data collection for future designs. Given their dimensions and high sensitivity, single-mode (SM) optical fiber sensors are a viable option. Distributed measurements along the length of the SM fiber are captured using optical backscattering reflectometry (OBR), where fluctuations in the density of the optical fiber core cause Rayleigh scattering. The technology demonstrates significant performance under high temperatures and supports the implementation of post-build embedded fiber sensing; pressurized embedding techniques create consistent strain and temperature measurement bridges to the fiber with independent thermal and mechanical data channels. This work demonstrates in-build LPBF/DMLM manufactured parts with embedded fiber and explores in-process measurements of laser-part interactions, effectively resolving static and dynamic temperature responses. A discrete thermal or stress load generates a response along the fiber, and the responses from a series of loads can be assembled to form the part's signature space. A new unknown load can be measured by projecting the OBR response into this space, with locally variable coupling allowing the stress and temperature to be differentiated. The paper presents the approach and provides several demonstrations.

1. Introduction

Structural health monitoring (SHM) has become increasingly critical in various industries, including aerospace and civil engineering, as the demand for high-performance, safety-critical components favors developing materials and structures [1]. Effective SHM is not only about detecting damage once it has occurred but also about understanding the onset and progression of damage. An accurate prognosis of damage allows for timely interventions and maintenance, significantly reducing the risk of catastrophic failures and extending the lifespan of structural components. Traditionally, SHM systems have relied on discrete sensors for post-failure diagnostics gauges [2, 3]. However, emerging needs for more proactive monitoring and control have driven the development of integrated sensor systems that provide real-time and distributed insight into the health of a structure.

Integrating sensors in structural components can offer a promising platform to evaluate loads and environmental conditions before damage manifests, facilitating more informed and timely interventions. This is particularly vital in high-performance applications where failure can have severe consequences. Additive manufacturing (AM) has emerged as a fabrication method to create complex geometry and customized components optimized for high temperatures and

extreme conditions [4]. Integrating sensors into these additively manufactured parts will enhance operational reliability and safety.

Optical fiber sensors present a promising platform for this purpose due to their inherent advantages. Optical fibers are versatile due to the material's designed optical properties (low losses over long distances), immunity to electromagnetic interference, lightweight construction, compact dimensions, and ability to accommodate distributed sensor systems [5]. Consequently, optical fiber is increasingly employed for real-time monitoring of in-process and fabricated materials, providing distinctive capabilities for quality control and performance assessment along the length of the fiber [6]. Optical fibers can map various physical parameters, including temperature, strain, acoustic vibrations, electric current, and pressure, by detecting changes in light propagation and scattering that result from localized strain profiles along the fiber [7]. This capability to capture strain (both mechanical and by thermal expansion) along the length of the optical fiber enables in-situ monitoring during and post-process. Subtle changes to the design of AM parts allow optical fiber to be embedded into a part to optimize for capturing strain and temperature fields. The bonding application of an optical fiber into an AM part is critical to discriminate between strain and temperature loads. This method has been previously demonstrated in PLA 3D-printed warren truss structures where optical fiber was embedded with and without an applied adhesive to demonstrate accuracy variances from an applied heat load and three-point bend test [8].

Integrating optical fiber sensors into manufactured components, particularly metal components, is valuable due to metal's use in aerospace and defense applications. Optical fiber technology has been integrated into various manufacturing processes, such as ultrasonic additive manufacturing (UAM), selective laser melting (SLM), directed energy deposition (DED), and laser powder bed fusion (LPBF). Significant progress has been achieved with UAM processes for creating aluminum parts [9,10]. Additionally, embedded optical fiber sensors with electroplated metal coatings have been included in SLM parts made from stainless steel and other metal alloys [11,12]. In the case of DED, efforts have also led to incorporating embedded fiber sensors in titanium and Inconel alloys with metal coatings and using high-temperature adhesives [13, 14].

Additionally, optical fiber sensors have been shown to measure up to 700˚C and are still viable at lower temperatures after exposure to 1200˚C for several hours [15]. An adaptive reference scheme demonstrated by Sweeney et al. [16] shows the ability to have persistent high-temperature measurements up to 1000˚C using standard telecommunications optical fiber. This procedure was applied to a Ni/Cu bi-metallic coated optical fiber embedded in a stainless-steel 316 (SS316) matrix using L-PBF, where strains from the fiber were measured up to 1000˚C [17].

The integration of optical fiber in AM parts has been demonstrated in various processes. However, there remain challenges with optimizing the coupling fields post and during integration and its effect on the performance debits of the AM part. Also, the interpretation of the measurements along the length of the optical fiber has not been fully explored. The processing of this data will lead to capturing real-time 3D strain and temperature fields. The primary aim of this research article is to formulate a comprehensive set of guidelines geared towards accurately measuring temperature and strain for in-build and post-build AM parts. A demonstration capturing basis functions shows the ability to process

the distributed fiber data, and a technique will be demonstrated for decoupling strain and temperature with a post-build part. Lastly, real- time measurements with an integrated optical fiber in a Direct Metal Laser Melting (DMLM) E8 tensile test specimen are shown. The knowledge derived from these methodologies will be used for future characterization of in-build and post-build integration of optical fiber and its effect on the performance of the part.

2. Measurement Method

2.1. Optical Frequency Domain Reflectometry

The experimental optical fiber measurements were processed using Optical Frequency Domain Reflectometry (OFDR), which uses optical backscattering reflectometry (OBR) to interrogate real-time, distributed measurements. This method commonly employs a tunable laser source (TSL) that emits a continuously changing wavelength within the c-band spectrum over time. The light emitted by this laser source is split into two paths: one for measurement and the other for reference. In the measurement path, the light is coupled into the optical fiber sensor, interacting with the optical fiber's natural inhomogeneities, leading to Rayleigh backscattering. This backscattered light serves as the returning signal. Conversely, the light is directed to a beam splitter in the reference path, where the scattering profiles from the measurement and reference arms are collected to create interference. Subsequently, these two scattering profiles are cross correlated to assess their similarities, primarily based on the spectral shifts observed. This correlation process translates into strain and temperature measurements using calibration coefficients that have been empirically determined [18,19,20].

An ODiSI 6100 series interrogator was used for all distributed optical fiber measurements based on OBR. This interrogator measures the recorded spectral shift responses from the intrinsic Rayleigh backscattering signal within an Au/Cu-coated optical fiber. These recorded shifts corresponded to variations in both temperature and strain. The concept of spectral shift is described as follows:

$$\frac{\Delta\lambda}{\lambda} = \frac{\Delta\nu}{\nu} = K_T \Delta T + K_\varepsilon \Delta\varepsilon \tag{1}$$

In this equation, K_T represents the sum of the thermal expansion and thermo-optic coefficients. Typical values for these coefficients in Germania-doped silica core fibers are $0.55\times10^{-6}°C^{-1}$ and $6.1\times10^{-6}°C^{-1,}$ respectively. The strain coefficient, Kε, depends on factors such as group index, strain optic sensor components, and Poisson ratio, resulting in a value of 0.787 [21]. Consequently, when measuring temperature, the strain coefficient is disregarded, allowing for the measurement of spectral shifts using the known constant to determine temperature and vice versa with strain. The strain can directly relate to the spectral shift for embedded optical fiber without an applied temperature.

$$\varepsilon = -0.667 \cdot \Delta\nu \tag{2}$$

An optical fiber that is not embedded experiences only the effects of an applied temperature; this change is related to Eq. 3.

$$\Delta T = -0.638 \cdot \Delta \nu \tag{3}$$

3. Basis Function Projection Demonstration

3.1 Experimental Setup

A single-mode telecommunication optical fiber (Corning) with a 9 µm core and 125 µm silica cladding surrounded by acrylate coating was attached to a 101.6 mm × 66.7 mm × 0.75 mm stainless steel sheet. The optical fiber was secured using Kapton tape and oriented in an arbitrary sinusoidal pattern. Heat loads were applied on the opposing side of the fiber using a 1070 nm fiber laser (IPG YLR-500-AC) and a Galvo Scanner (ExcelliSCAN14). The optical fiber was interrogated with a spatial resolution of 0.65 mm, so for this sample, there were 290 temperature points along the length of the optical fiber on the sample. Fig. 1 shows the fabricated sample with the attached optical fiber and a schematic demonstrating the measured temperature profile from an applied heat load.

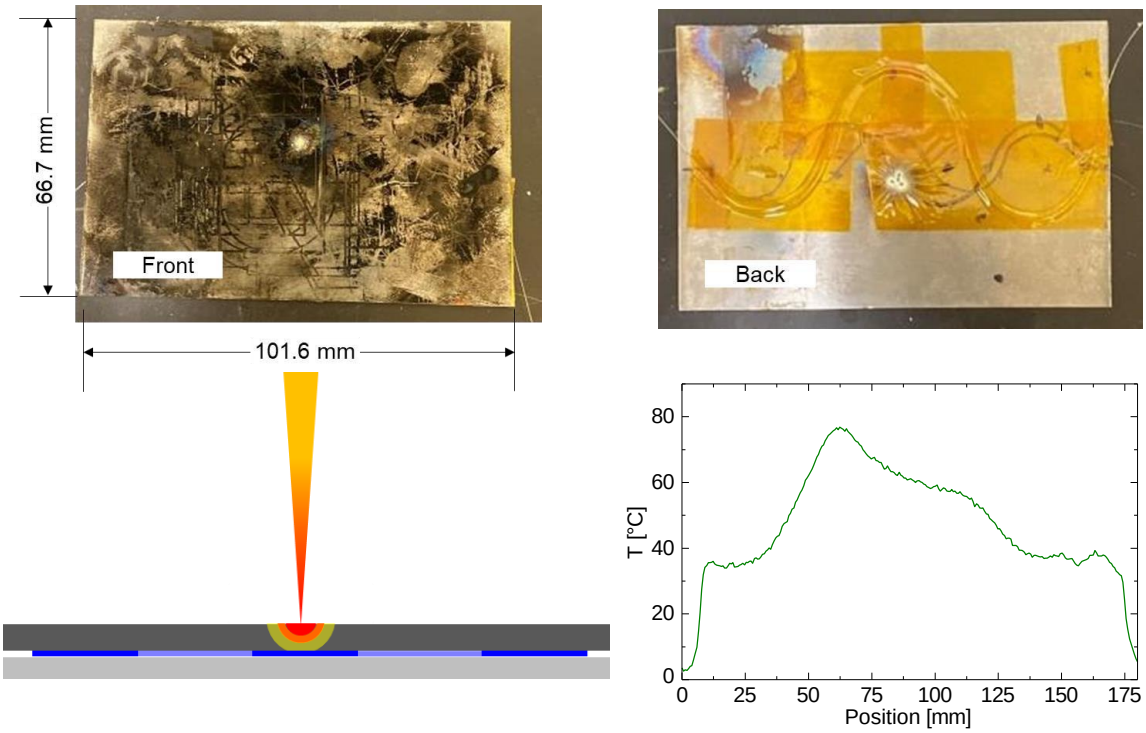

Fig 1. A surface-bonded stainless-steel sheet with single-mode optical fiber sensors and a schematic demonstrate the response to an applied heat load.

3.2 Capturing Unique Basis Functions

Using the stainless-steel sample with attached optical fiber, 25 unique steady-state temperature profiles were measured using the IPG fiber laser at a power output of 30 W. Each point was spaced 5 mm apart to create a 5×5 grid of points based on an arbitrary set of coordinates established on the sheet. The thermal resistance based on each steady-state temperature measured for each location shows a unique profile (refer to Fig. 2)

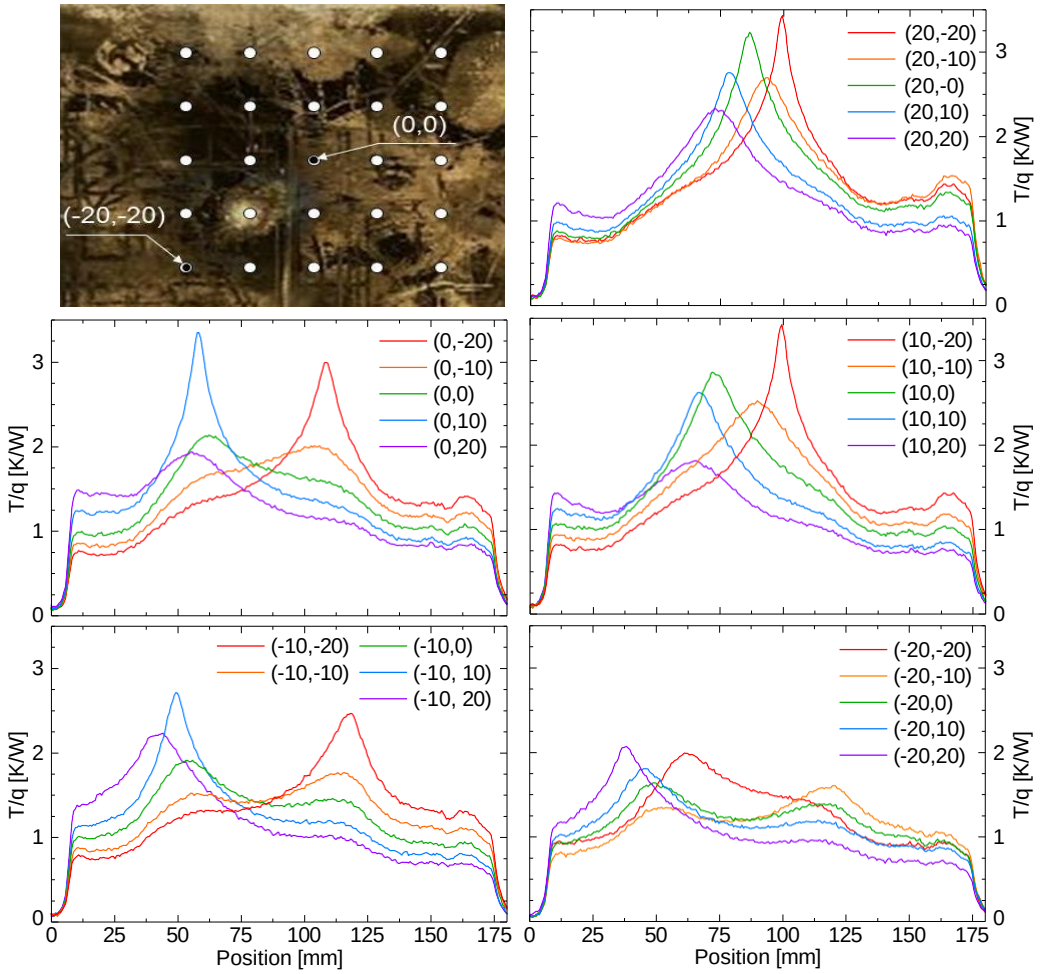

Fig 2. Thermal resistance measured for each arbitrary location from the integrated stainless-steel sample

The data captured in Fig. 2 gives the ability to capture 3D field data by taking advantage of the principle of superposition. For example, the heat diffusion equation governs the temperature field within a part. When a load is applied to the part, the resulting increase in temperature can be added to the existing profile. When multiple heat loads are applied, the resulting temperature is the superposition of all the heat loads. A matrix can be generated by exciting a part at discrete locations. The temperature change along the fiber will be recorded to create columns of $\mathbf{A}_{\mathbf{NxM}}$ where N is the temperature points along the length of the optical fiber, and M is the number of positions captured. Once matrix $\mathbf{A}$ has been generated, the equivalent heat load can be found using Equation 4.

$$\mathbf{q} = \left(\mathbf{A}^T\mathbf{A}\right)^{-1}\mathbf{A}^T \cdot \Delta\mathbf{T} = \mathbf{B} \cdot \Delta\mathbf{T} \tag{4}$$

The number of heat loads M cannot exceed the number of gauge sections along the length of the optical fiber N. To demonstrate this, nine steady-state temperature rises from the applied IPG

fiber laser were captured ($\mathbf{A}_{290x9}$). Discrete heat sources (ΔT) from sub-basis functions on 1 mm increments were captured (refer to Fig. 3)

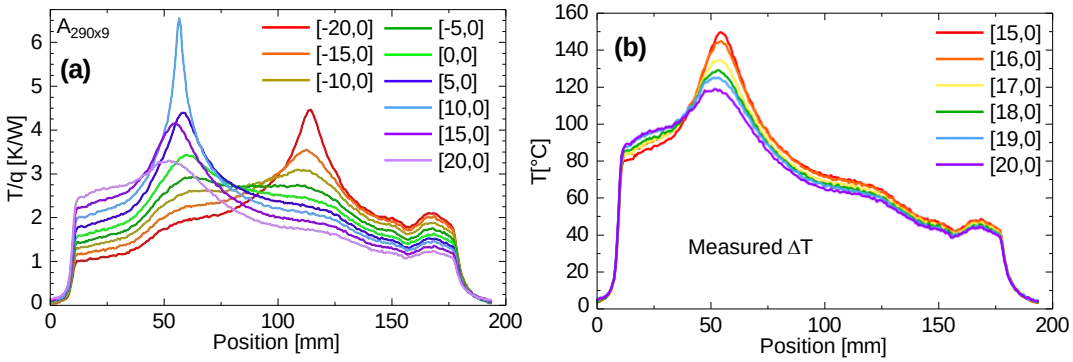

Fig 3. (a) Temperature profile along the fiber for heat loads applied at different locations on the stainless-steel sheet and (b) temperature changes (ΔT) on 1 mm increments

The temperature profiles captured in Fig. 3a constructed the **A** matrix, and the equivalent heat load was analyzed for each ΔT applied every 1 mm for a sub-section on the stainless-steel sheet. The heat loads were resolved using Eq. 4, and the results show the magnitude relative to two trained data points in the **A** matrix, in this case being (20,0) and (15,0) (refer to Fig. 4)

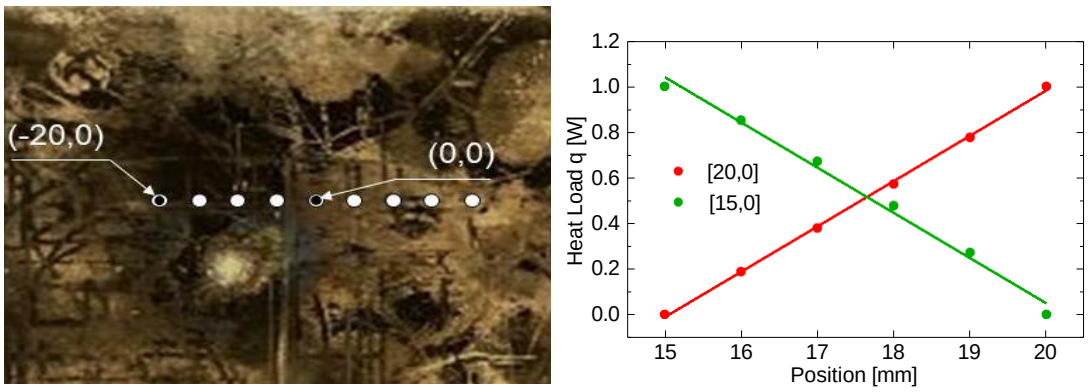

Fig 4. Heat sources recovered from each temperature profile are shown in Fig 3b. using Eq. 4.

This approach can also be used to analyze 3D strain fields. A part will be subjected to a discrete force and equipped with two fiber types. One fiber is thermally coupled to the part but not mechanically, while the other is thermally and mechanically coupled. Applying thermal and mechanical loads to the part can capture temperature and strain fields. However, there are limitations to the placement of these fibers. For instance, if a fiber runs straight through the center of the part, the resulting matrix **A** will be non-invertible. Similarly, if a sinusoidal fiber is placed along the neutral axis of the part, it will exhibit minimal strain response, leading to a singular matrix.

4. Decoupling Strain and Temperature

4.1 Post-Build: Adhesive Injection Method

The uniformity of the bonding mechanisms affects the sensitivity to mechanical and thermal loads. A method for applying a uniform adhesive was demonstrated on 3D PLA-printed E8 tensile test specimens with sinusoidal channels running along the samples. Included in the 3D prints were luer lock attachments that funneled into the sinusoidal channels throughout the length of the specimen. Standard telecommunications optical fiber was coiled into a syringe ($\Phi \sim 25.4$ mm) and threaded through the plastic E8 bar. An instant low-viscosity (~450cP) adhesive (LOCTITE 380) was injected into the larger syringe. The syringe was secured to the attached luer lock, where applying a small amount of pressure enabled the adhesive to coat the sinusoidal channel uniformly. The setup before injection of the adhesive can be seen in Fig. 5. Additionally, to check the uniformity along the length of the plastic E8 bar, varying cross sections were made using a diamond saw to expose the channel and optical fiber laying in the channel. Micrographs were captured to demonstrate this application technique (refer to Fig. 6)

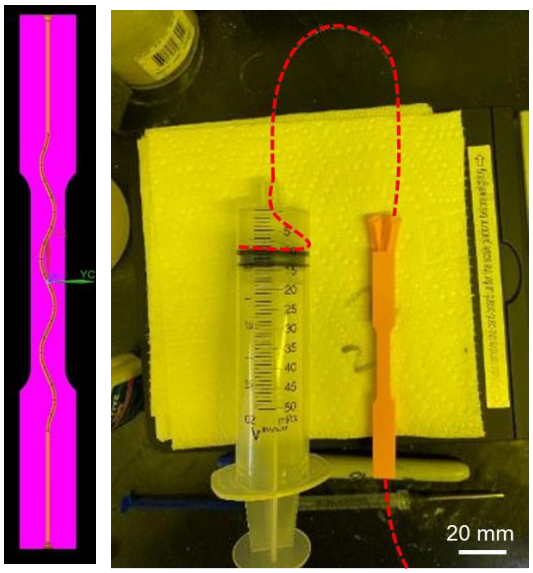

Fig 5. Injection technique using an attached luer lock for pressurized application of an adhesive demonstrated on plastic E8 tensile test specimen

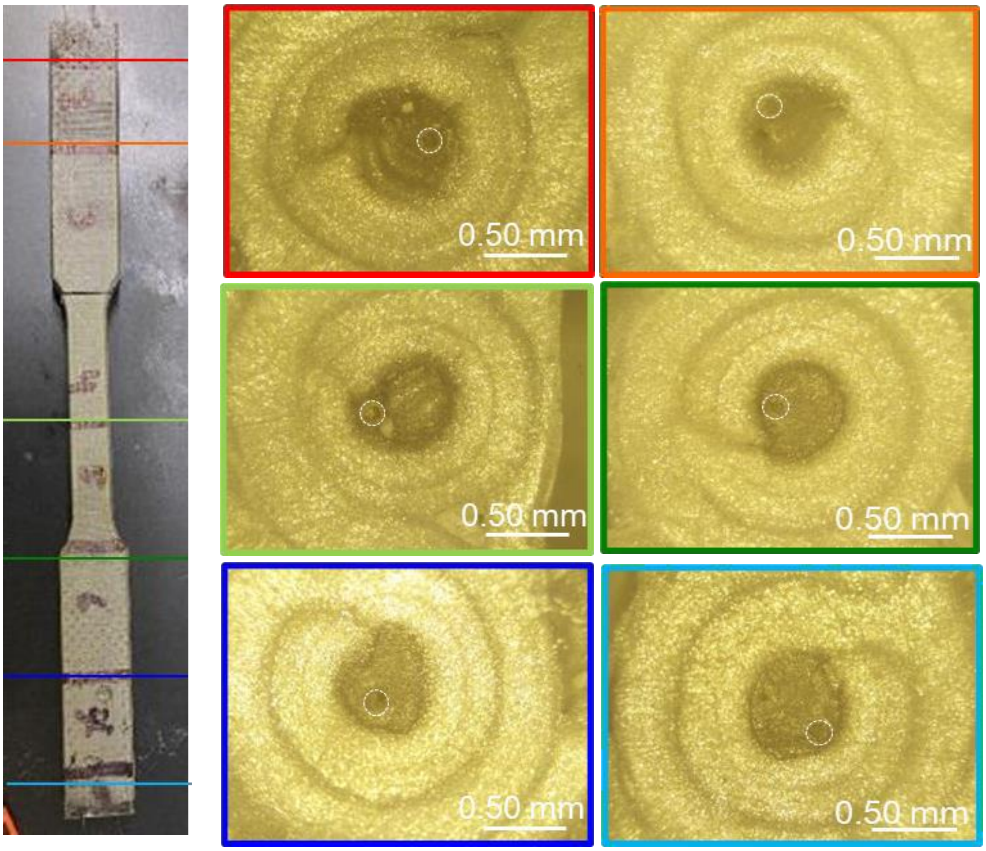

Fig 6. Micrographs along a plastic E8 tensile test specimen showing the uniformity of the applied adhesive and orientation of the optical fiber in the channel

This same technique was applied with a silicon carbide high-temperature resistant adhesive (Ceramabond 890), which has a medium to high viscosity (35,000 – 55,000 Cp) and showed the same uniformity along the length of the sinusoidal channel. These plastic E8 bars were for demonstration purposes. However, this pressurized application approach can be applied similarly to metals by integrating threads onto the fabricated parts to attach a luer lock.

4.2: Post-build: Strain Testing

A plastic 3D-printed E8 tensile test specimen was used to evaluate the strain response when subjected to a tensile load. A single standard telecommunications optical fiber was threaded through two channels. Using the pressurized application method, one channel was secured with LOCTITE 380, a low-viscosity adhesive. Graphite powder was injected into the other channel to act as a lubricant for the optical fiber. The applied tensile load was conducted using a Mark-10 UTM, and the distributed strain profile for each fiber segment embedded in the part was measured in real-time. The plastic E8 bar was loaded at 0.01 mm/s until the sample fractured. The resulting strain as a function of time shows that the optical fiber secured using the adhesive is more sensitive to an applied strain than the other bridge application using graphite powder. The setup of the plastic E8 tensile test specimen secured in the UTM and the strain for varying applied tensile loads is shown in Fig. 8.

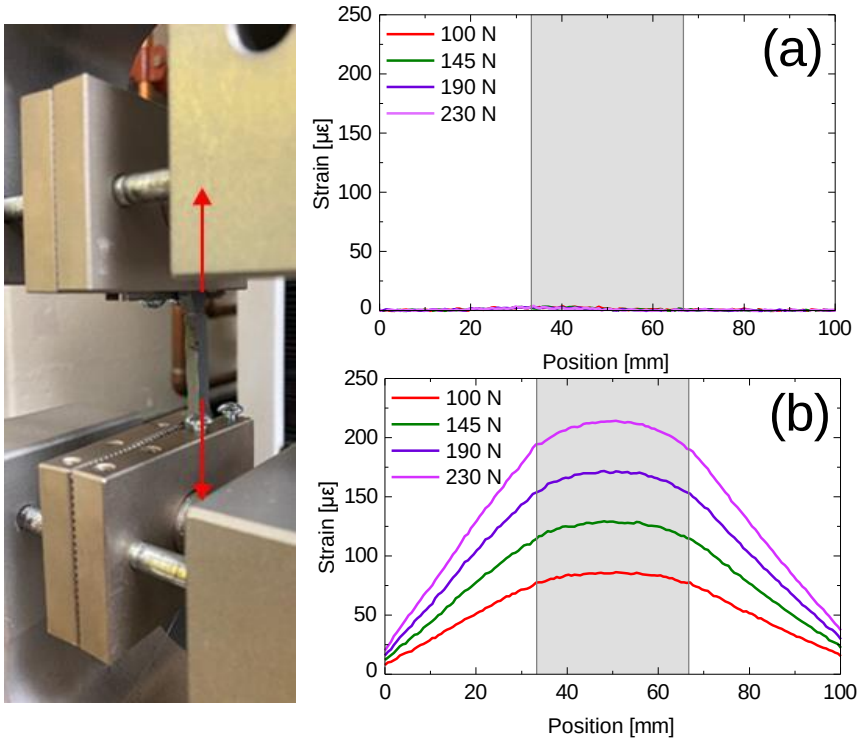

Fig 8. In-situ distributed optical fiber strain measurements from two channels with applied a) graphite powder and b) LOCTITE 380 adhesive using attached luer locks

The in-situ strain measurements for each channel provide insight into the evolution of the response in real time. Like Fig. 8, During the entire duration of the tensile test, the graphite injected channel was insensitive to the applied load (refer to Fig. 9)

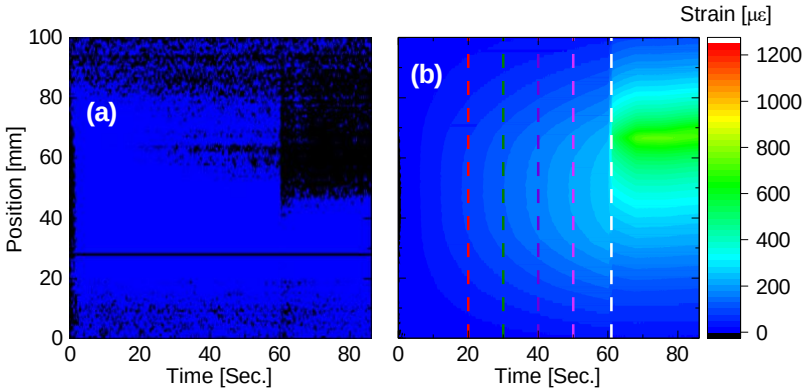

Fig 8. In-situ distributed optical fiber strain measurements were applied during tensile loading for two channels: a) graphite powder and b) LOCTITE 380 adhesive using attached luer locks. The white dotted line shows the instant the specimen fractured

4.3: Post-build: Temperature Testing

In-situ temperature measurements along a plastic E8 tensile test specimen were captured to evaluate the dependence on the mechanical and thermal bridge. A temperature test was performed for one integrated E8 bar, where a heat load was applied from a hot plate (Corning PC-400D). The temperature was limited to 80˚C, given that the part would start to deform plastically. Like the previous strain experiment, a single optical fiber was threaded through two sinusoidal channels, where one was secured using adhesive and the other was lubricated with graphite powder. The hot plate had three different setpoints and was compared with a thermal camera (Optris PI-640i) and three thermocouples attached to the surface (OMEGA Data Logger). The experimental setup and schematic are shown in Fig. 9

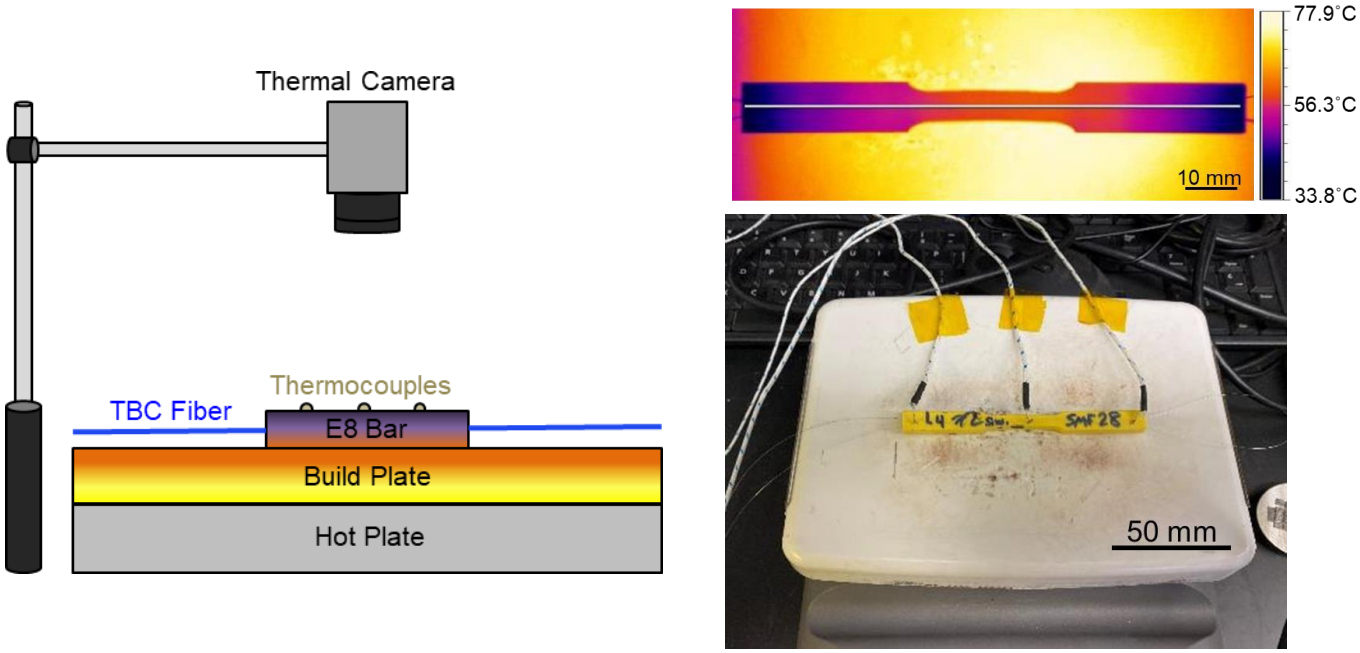

Fig 9. Experimental setup and schematic of integrated plastic E8 bar on a hotplate with attached thermocouples and thermal camera

The in-situ temperature profile for each channel was evaluated with an increase in temperature set by the hotplate (40˚C, 60˚C, and 80˚C). The mechanically coupled optical fibers' spectral shift measurements were transduced to a temperature measurement using Eq. 3. However, the distribution profile was a combination of additional strain due to the plastic deformation. The alternative channel with graphite powder shows good agreement compared to the thermal camera and thermocouples and was insensitive to the added strain caused by the part mechanically deforming (refer to Fig. 10).

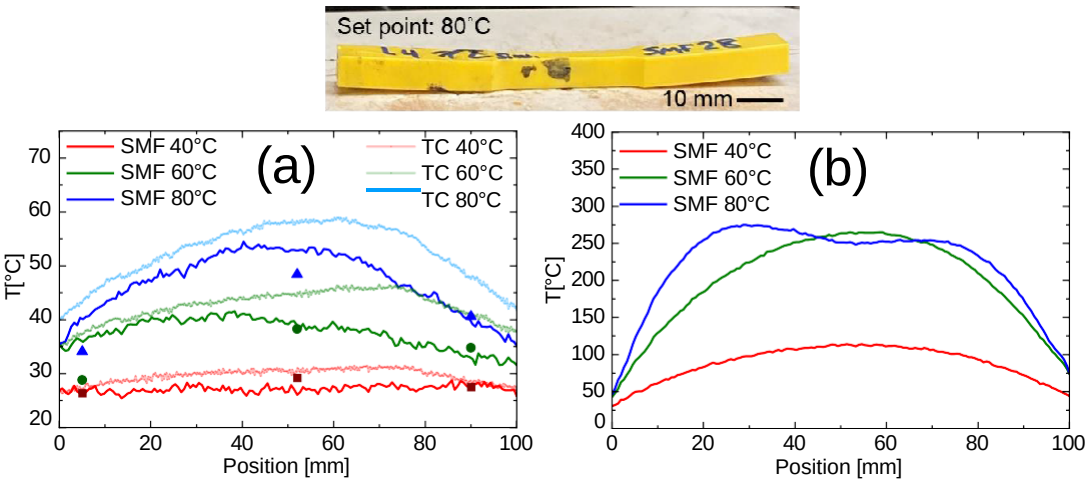

Fig 10. In-situ distributed optical fiber temperature measurements from heat load applied from hotplate for channels with a) graphite powder and b) LOCTITE 380 adhesive using attached luer locks

The thermal camera's measurement is larger than the temperature measurement transduced from the in-situ optical fiber. This is due to the calibration of the emissivity of the thermal camera. Additionally, the distributed temperature profile at 80˚C does not show the plastic deformation of the E8 tensile test specimen, which shows it can scale linearly with temperature. Comparing the maximum temperature for each of the three sensors at each setpoint, the embedded optical fiber with graphite powder linearly scales with the thermocouples and thermal camera (refer to Fig. 11)

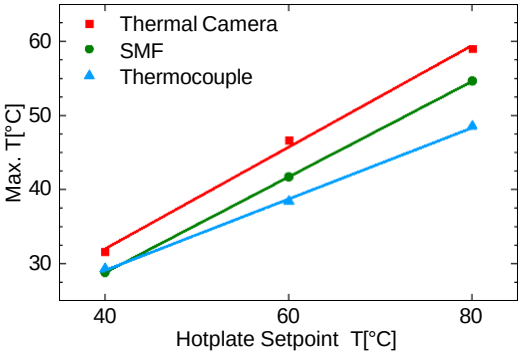

Fig 11. Maximum temperature from the embedded optical fiber, thermocouples, and profile captured using the thermal camera with each setpoint on the hotplate

It was demonstrated that strain and temperature can be decoupled for low-temperature cases for plastic E8 parts. The following steps will involve applying this application technique to metal E8 bars. Temperature and strain accuracy measurements will be evaluated, and their limitations in terms of viability and when the bridge application failures for the mechanically bonded optical fiber will be assessed.

5. DMLM In-Process Embedding

5.1 Real-Time Measurement During Build

All direct metal laser melting (DMLM) processing was performed in a commercial M2 Series print at GE Aerospace Research, Niskayuna. Channels were designed into the DMLM-built structure to place Au/Cu coated optical fiber, as shown in Fig 12(a). First, 3 mm of material was built, and a single 1 mm diameter sinusoidal channel running throughout the length of the E8 tensile test specimen was formed. When complete, the metal powder was removed and cleaned from the build plate, and then a thermal barrier-coated (TBC) Au/Cu optical fiber was placed into the channel. The TBC was applied using low thermal conductivity powder and put in a syringe, where the fiber was drawn through the needle to coat the optical fiber uniformly. This prepared optical fiber was placed within the designed channel, and the rest of the DMLM process was continued. Another 3 mm of material was printed above the optical fiber to create an E8 bar with embedded optical fiber.

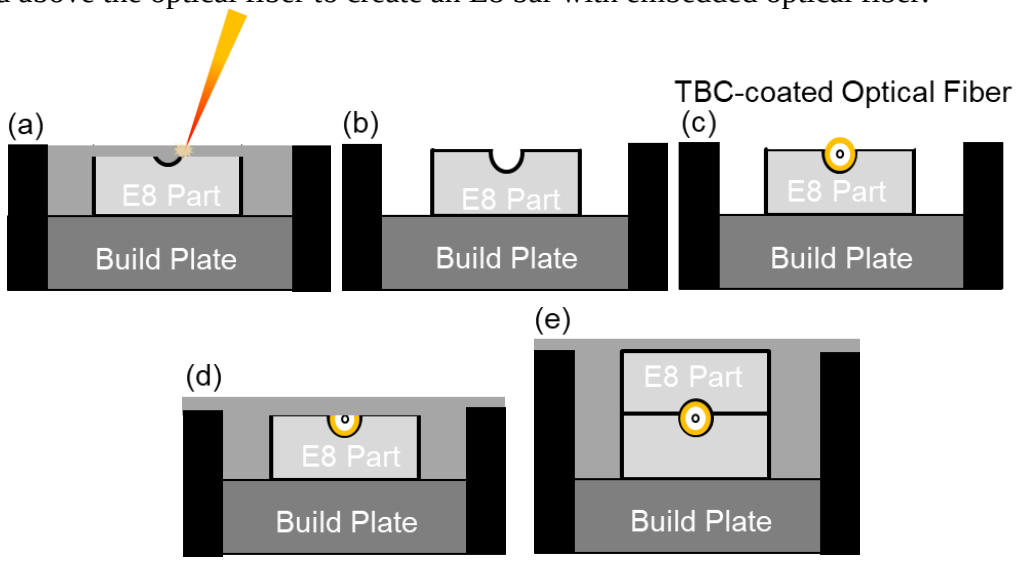

Fig 12. Integration of Au/Cu coated optical fiber into DMLM build. (a) The first 3 mm of material is built up with a 1 mm channel (b), and once complete, the remaining metal powder is cleaned off the build plate and E8 part. (c) Then, a TBC is applied to the optical fiber and placed in channel (d), and another layer of powder is pushed on top of the sample to continue the process. (e) Another 3 mm of material is built on top of the optical fiber to complete the build

During the integration process, the optical fiber placed into the E8 bar was spliced to an LC/APC connector, where it was interrogated using the ODiSI 6100 series system. The egress portion of the optical fiber was terminated using index-matching gel to prevent back reflections. The optical fiber was measured at 32 Hz, with a spatial resolution of 0.65 mm. The spectral shift signal during the build was transduced to a temperature measurement using Eq. 3. The position along the optical fiber and the resulting temperature from the spectral shift signal during the DMLM build are shown in Fig. 12.

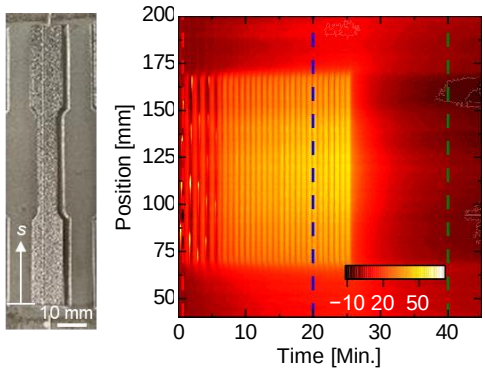

Fig 12. In-situ spectral shift measurements during DMLM build transduced to temperature measuring using Eq. 3.

Fig. 12 shows a significant peak in the first four layers since the material is deposited directly onto the optical fiber's sinusoidal path. The spectral shift signal stabilizes as the DMLM process continues, and the deposited layers move further away from the embedded optical fiber. Since the optical fiber is embedded, the spectral shift measurement was transduced into both measurements using Eq. 2 and 3. It is expected that there is residual stress within the part as the material is being melted and cooled down, so the measurement is not purely temperature or strain. The maximum signal for each layer is shown in Fig. 13 throughout the entire print. Additionally, the variances in the signal are captured at 40 seconds into the build, 20 minutes, and, when complete, are shown to capture the evolution of the signal. Fig. 14 shows a slight shift after the build finishes and cools, attributed to residual strain within the part.

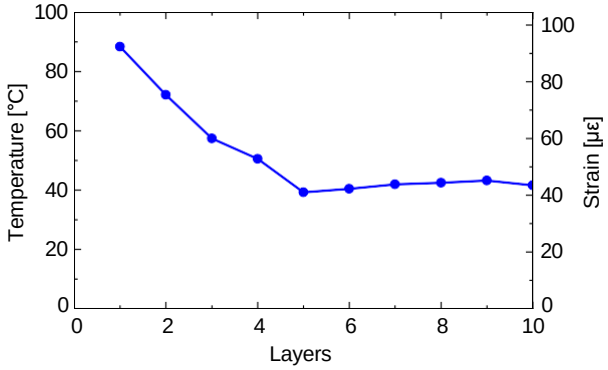

Fig 13. Maximum in-situ spectral shift measurement converted to temperature and strain for each printed layer during the DMLM build

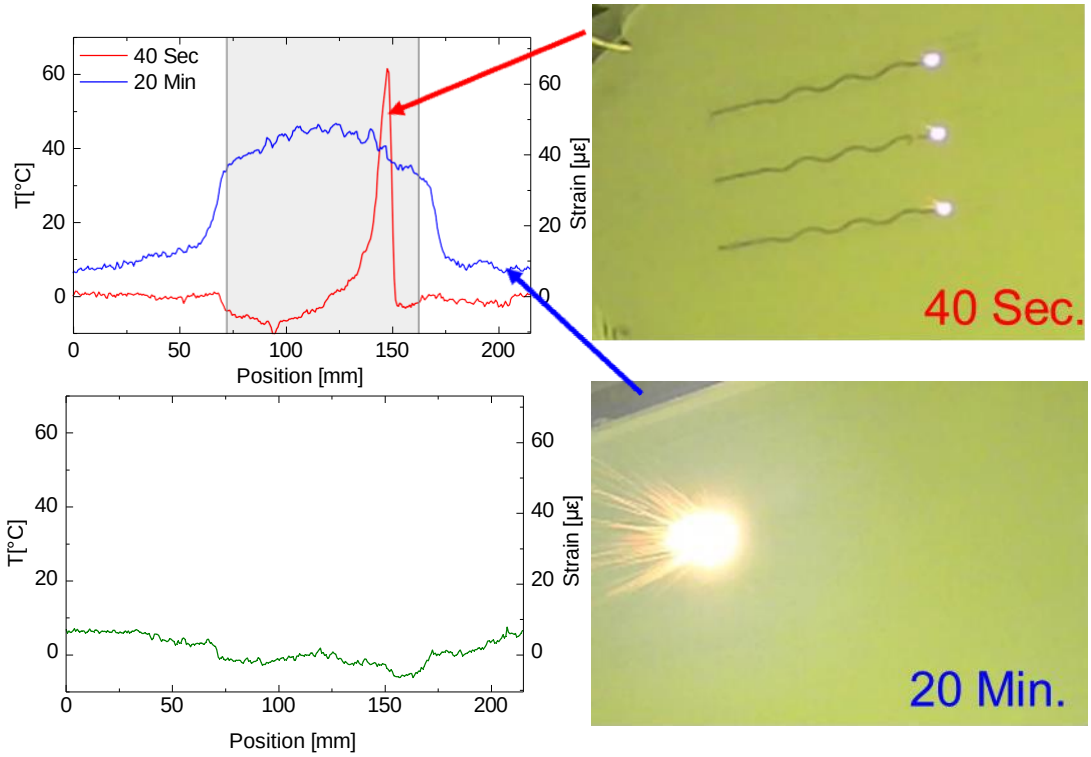

Fig 14. In-situ spectral shift measurements during and post-process for a DMLM build transduced to temperature and strain

5.2 Dynamic Temperature Response

The dynamic temperature response post-build from the interrogated E8 tensile test specimen was captured. Heat loads were applied at a power of 200W and a pulse rate of 100 ms for discrete points on the E8 bar. Like what was shown from capturing static basis functions, the same principle can be applied in the transient state to resolve discrete heat loads. The maximum in-situ spectral shift measurement converted to temperature is shown in Fig. 15. This is the instantaneous peak before the signal dissipates and shows proof of concept in terms of having a unique signal based on the position along the metal E8 part.

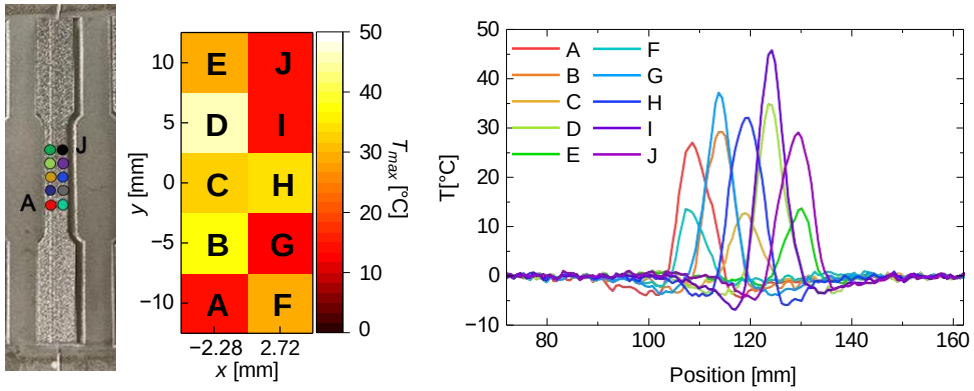

Fig 15. Maximum in-situ spectral shift measurement converted to temperatures using Eq. 3. At discrete points on metal E8 post-build

The linear response to changes in the power output and the pulse rate were evaluated for two positions on the E8 bar. The peak spectral shift responses scale linearly with increases in both parameters. The power output from 200-400W (200 ms) and pulse rate from 100-400 ms (200 W) were evaluated. (refer to Fig. 16)

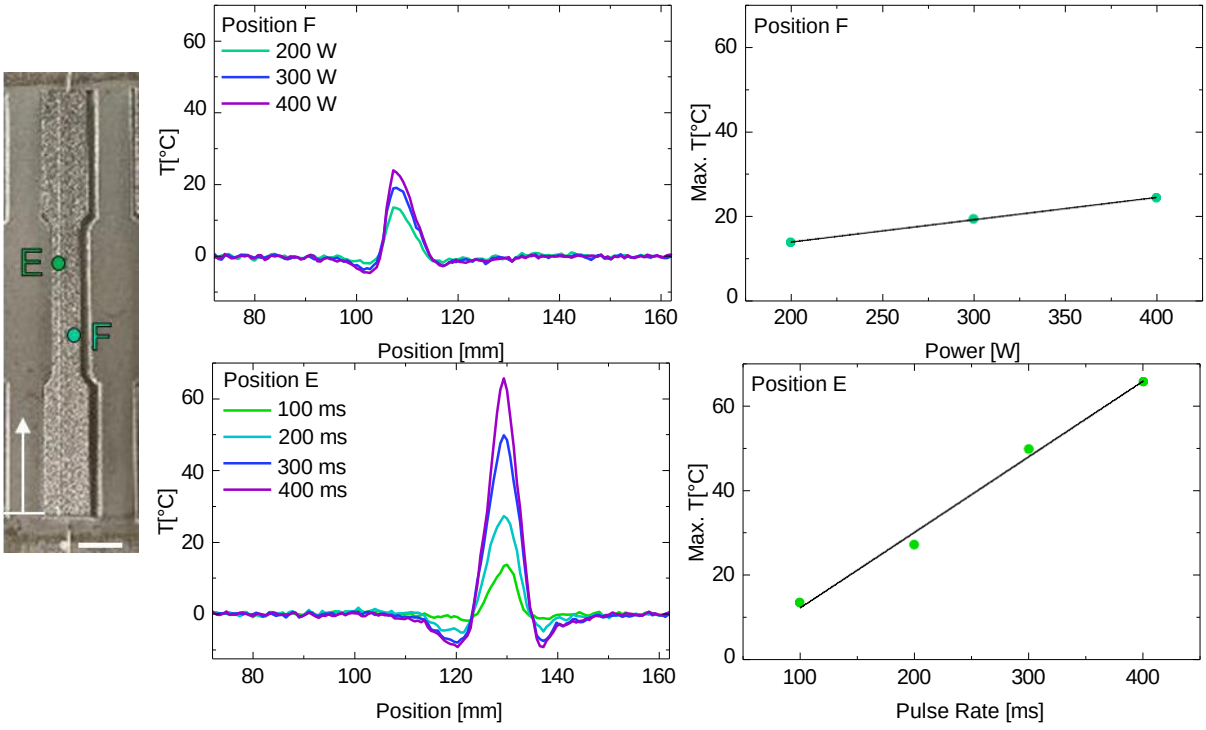

Fig 16. Maximum in-situ spectral shift response converted to temperature based on changes to power output and pulse rate for two different positions on a post-built DMLM E8 bar

The dynamic and static response from heat loads has been demonstrated to show position-dependent temperature profiles. Using the principles of superposition, parts fabricated with

optical fiber have the potential to resolve unknown heat and strain loads, given the part is trained. Future steps will include integrating optical fiber into a DMLM part to resolve unknown static heat loads, and an optimal approach for dynamic loads needs to be established.

6. Conclusions

The integration of optical fiber distributed sensing using OFDR techniques in combination with Additive manufacturing (AM) presents a promising avenue for developing smart parts. This combination enables the creation of minimally invasive sensors with selective coupling, allowing for precise temperature and strain measurement. The accuracy and data quality achieved facilitates the projection of the measured responses into a vector space defined by known loads. The technology demonstrates robust performance under high temperatures and supports post-build embedded fiber sensing. Pressurized embedding techniques ensure consistent strain and temperature measurement bridges to the fiber while providing independent thermal and mechanical data channels. This work demonstrates in-build LPBF/DMLM with embedded fiber. It also explores in-process measurements of laser-part interactions, achieving resolution in static and dynamic temperature responses. The following steps involve applying this post-build strategy to metal parts to evaluate and refine the approach. Further research will focus on studying the mechanics of strain and temperature bridges as influenced by the type of fiber and adhesive applied. Additionally, efforts will be directed toward assessing the accuracy of various application methods and expanding the technology to accommodate more complex geometries.

7. References

[1] Y. Liu, S. Nayak, "Structural Health Monitoring: State of the Art and Perspectives," *JOM* **64**, 789-792 (2012).
[2] S. Laflamme, M. Kollosche, V.D. Kollipara, H.S. Saleem, G. Kofod, "Large-scale surface gauge for health monitoring of Civil Structures," *SPIE 8347-8347IP* (2012).
[3] H. Rocha, C. Semprimoschnig, J.P. Nunes, "Sensors for process and structural health monitoring of aerospace composites: A review" *Engineering Structures* **237** 112231 (2021).
[4] N. Nordin, M. Johar, M. Ibrahim, O. Marwah, "Advances in High-Temperature Materials for Additive Manufacturing," *IOP Conf. Ser.; Mater. Sci. and Eng.*
[5] B. Lee, "Review of the present status of optical fiber sensors," *Optical Fiber Technology* **9**(2), 57-79 (2003).
[6] A. Rogers, "Distributed optical-fiber sensing," *Measurement Science and Technology* **10**(8), (1999).
[7] V.M. Murukeshan, P.Y. Chan, L.S. Ong, L.K. Seah, "Cure monitoring of smart composites using Fiber Bragg Gratings based embedded sensors," *Sensors and Actuators A: Physical* **79**(2), 153-161 (2000).
[8] B. Hlifka, E. Kinzel, "Distributed Optical Fiber Testing for Additive Manufacturing," *Solid Freeform Fabrication Symposium*, Austin TX Aug. (2023).
[9] A. Hehr, M. Norfolk, J. Wenning, J. Sheridan, P. Leser, P. Leser, J.A. Newman, "Integrating Fiber Optic Strain Sensors into Metal Using Ultrasonic Additive Manufacturing," *Additive Manufacturing of Composites and Complex Materials* **70**, 315-320 (2018).
[10] H.C. Hyer, D.C. Sweeney, and C.M. Petrie, "Functional fiber-optic sensors embedded in stainless steel components using ultrasonic additive manufacturing for distributed temperature and strain measurements," *Additive Manufacturing* **52** (2022).
[11] D. Havermann, J. Matthew, W.N. Mcpherson, R. J. Maier, D.P. Hand, "Temperature and Strain Measurements with Fiber," *Journal of Lightwave Technology* **33**(12), 2474-2479 (2015).
[12] J. Mathew, D. Havermann, D. Polyzos, W.N. Macpherson, D.P. Hand, R.J. Maier, "SS316 Structure Fabricated by Selective Laser Melting and Integrated with Strain Isolated Optical Fiber High-Temperature Sensor," *International Conference on Optical Fiber Sensors,* Curitiba (2015).
[13] R. Zou, X. Liang, R. Cao, S. Li, A. To, P. Ohodnicki, m. Burie, and K. Chen, "Embedding Distributed Temperature and Strain Optical Fiber Sensors in metal Components Using Additive Manufacturing," *Conference on Lasers and Electro-optics* San, Jose, CA (2018).
[14] E. N. Snider, R.K. Saha, C. Dominguez, J. Huang, and D.A. Bristow, "Embedding Fiber Optic Sensors in Metal Components via Direct Energy Deposition," *Solid Freeform Fabrication Symposium*, Austin TX Aug. (2023).
[15] B. Hlifka, E. Kinzel, "Distributed Single-Mode Optical Fiber High Temperatures Measurement," ASME Heat Transfer Summer Conference, Anaheim CA July (2024).
[16] D.C. Sweeney, A.M. Schrell, C.M. Petrie, "An Adaptive Reference Scheme to Extend the Functional Range of Optical Backscatter Reflectometry in Extreme Environments," IEEE Sensors **21**(1), 498-509 (2021).
[17] H.C. Hyer, C.M. Petrie, "Distributed strain sensing using Bi-metallic coated fiber optic sensors embedded in stainless steel", *Additive manufacturing* **91** 104335 (2024).
[18] Z. Ding, et al. "Distributed optical fiber sensors based on optical frequency domain reflectometry: a review," Sensors **18**(4), 1072 (2018).

[19] Kreger, et al. “Optical frequency domain reflectometry: principles and applications in fiber optic sensing,” Proc. SPIE 9852-98520T (2016).
[20] Kreger, S. “Distributed strain and temperature sensing in plastic optical fiber using Rayleigh scatter,” Proc. SPIE 7316, Fiber Optic Sensors and Applications VI, 73160A (2009).
[21] S.T. Kreger, D.K. Gifford, M.E. Froggatt, A.K. Sang, R. G. Duncan, M.S. Wolfe, B.J. Soller, “High-resolution distance distributed fiber-optic sensing using Rayleigh backscatter,” SPIE 65301R (2007).